Numerical Study of the Inhibition of Premixed and Diffusion Flames by Iron Pentacarbonyl

M. D. RUMMINGER,[†] D. REINELT,[‡] V. BABUSHOK, and G. T. LINTERIS*
National Institute of Standards and Technology, Gaithersburg MD 20899, USA

Iron pentacarbonyl ($Fe(CO)_5$) is an extremely efficient flame inhibitor, yet its inhibition mechanism has not been described. The flame-inhibition mechanism of $Fe(CO)_5$ in premixed and counterflow diffusion flames of methane, oxygen, and nitrogen is investigated. A gas-phase inhibition mechanism involving catalytic removal of H atoms by iron-containing species is presented. For premixed flames, numerical predictions of burning velocity are compared with experimental measurements at three equivalence ratios (0.9, 1.0, and 1.1) and three oxidizer compositions (0.20, 0.21, and 0.24 oxygen mole fraction in nitrogen). For counterflow diffusion flames, numerical predictions of extinction strain rate are compared with experimental results for addition of inhibitor to the air and fuel stream. The numerical predictions agree reasonably well with experimental measurements at low inhibitor mole fraction, but at higher $Fe(CO)_5$ mole fractions the simulations overpredict inhibition. The overprediction is suggested to be due to condensation of iron-containing compounds since calculated supersaturation ratios for Fe and FeO are significantly higher than unity in some regions of the flames. The results lead to the conclusion that inhibition occurs primarily by homogeneous gas-phase chemistry.

INTRODUCTION

A worldwide ban on the production of the principal halogenated fire suppressants, including halon 1301 (CF_3Br), has created a need for new, environmentally acceptable fire suppressants; however, an agent with all of the desirable properties of CF_3Br is proving difficult to find. Understanding the inhibition mechanisms of known, effective flame inhibitors will help direct the search.

Certain metallic compounds have been found to be substantially more effective flame inhibitors than halogen-containing compounds [1–3]. In particular, iron pentacarbonyl ($Fe(CO)_5$) was found to be one of the strongest inhibitors—up to two orders of magnitude more effective than CF_3Br at reducing the burning velocity of premixed hydrocarbon/air flames [4, 5]. Although $Fe(CO)_5$ is highly toxic and flammable, understanding its inhibitory effect could lead to development of effective nontoxic agents.

The first detailed experimental studies of flame inhibition by iron pentacarbonyl are the studies of Wagner and coworkers [1, 4, 5]. Iron pentacarbonyl's inhibition action was studied by measuring the burning velocity of premixed flames with inhibitor added to the reactants [5]. In that research, Bonne et al. found $Fe(CO)_5$ to be significantly more effective than Br_2 in premixed hydrogen/air and n-hexane/air flames and found that its inhibition effectiveness decreased as the pressure was reduced below atmospheric. They also measured the emission intensity and absorption of Fe and FeO at various heights in a low-pressure (0.079 atm) flat premixed flame. Experiments of Lask and Wagner [1] showed that $Fe(CO)_5$ was more effective at reducing flame speed in hydrocarbon/air flames than in hydrogen/air flames, and more effective in hydrocarbon/air flames than in hydrocarbon/oxygen flames.

Reinelt and Linteris [6] studied the flame inhibition effect of iron pentacarbonyl in premixed flames by measuring the burning velocity, and in counterflow diffusion flames by measuring the extinction strain rate. In the premixed flames, behavior at low and high $Fe(CO)_5$ mole fractions was distinctly different: at low $Fe(CO)_5$ mole fraction the burning velocity was strongly dependent on inhibitor mole fraction, whereas at high $Fe(CO)_5$ mole fraction, the burning velocity was nearly independent of in-

*Corresponding author.
[†]National Research Council/NIST postdoctoral fellow.
[‡]Currently with BASF Aktiengesellschaft, 67056 Lüdwigshafen, Germany.

COMBUSTION AND FLAME 116:207–219 (1999)

Published by Elsevier Science Inc.
0010-2180/99/$19.00
PII S0010-2180(98)00033-9

hibitor mole fraction. In the counterflow flames, the degree of inhibition depended upon the location of the flame relative to the stagnation plane, as well as the location of the inhibitor addition. In a methane/air flame, little change in extinction strain rate resulted from addition of the $Fe(CO)_5$ to the fuel stream. In contrast, when $Fe(CO)_5$ was added to the oxidizer stream the inhibition was strong for low $Fe(CO)_5$ mole fractions, and the rate of extinction strain rate decrease was lower as the inhibitor mole fraction increased—but did not go to nearly zero as in the premixed flames. Reduction in extinction strain rate occurred for $Fe(CO)_5$ mole fraction up to 500 ppm (all uses of ppm in this paper signify mole fraction $\cdot 10^6$). A critical part of the research on $Fe(CO)_5$ is to understand iron pentacarbonyl's diminishing effectiveness at high mole fraction in order to avoid similar behavior in future fire suppressants.

Despite the experimental work performed to date, the inhibition mechanism of $Fe(CO)_5$ has not been thoroughly described. For example, the relative effects of homogeneous and heterogeneous chemistry have not been conclusively determined, although each has been suggested [1, 5, 7]. Heterogeneous effects are of interest because $Fe(CO)_5$ can form condensed-phase particulates upon heating [8, 9]. In premixed flames, some authors found that particles are formed upstream of the flame [10] whereas others observed particles only downstream of the flame [11] or did not comment on the location of the particles [5, 12, 13]. There exist conflicting claims in the literature as to whether a homogeneous or a heterogeneous mechanism is responsible for the inhibition. Since particles do not form at all flame conditions, and since the inhibition action in premixed flames is strong at low mole fraction and levels off with increasing inhibitor mole fraction [6], it is consistent that the inhibition may be through homogeneous reactions at low inhibitor mole fractions and heterogeneous reactions at high inhibitor mole fractions as was suggested by Jost et al. [4]. If particulates play a key role in the inhibition, then the search for halon alternatives could be directed toward chemicals that produce similar condensed-phase compounds.

Recently, Babushok and coworkers [14] have modeled the effect of an ideal gas-phase flame inhibitor by assigning nearly gas-kinetic rates to a set of plausible radical-scavenging and inhibitor-regenerating reactions. Comparison of the measured burning velocity of flames containing $Fe(CO)_5$ with the calculated burning velocities of flames containing an equal mole fraction of the ideal inhibitor showed that $Fe(CO)_5$ (at low initial mole fraction) performs nearly as well as the ideal inhibitor. Considering this result, the authors argued that the $Fe(CO)_5$ inhibition mechanism is dominated by homogeneous gas-phase chemistry.

The goal of the present paper is to examine the extent to which a homogeneous catalytic radical recombination mechanism for $Fe(CO)_5$ can reproduce experimentally determined premixed flame burning velocities and counterflow diffusion flame extinction strain rates, and to understand the features of such a mechanism. Results of numerical simulations of one-dimensional premixed flames of various mixtures of methane, oxygen, nitrogen, and iron pentacarbonyl are presented and compared with experimental measurements. The numerical results are analyzed to provide insight into the inhibition mechanism. Calculated extinction strain rates of counterflow diffusion flames are compared with experimental measurements for cases in which the inhibitor is added to the fuel or air stream. The condensation of iron compounds and formation of particulates in the flames are briefly discussed.

MODELING APPROACH

One-dimensional freely-propagating premixed flames are simulated using the Sandia flame code *Premix** [15], the *Chemkin* subroutines [16], and the transport property subroutines [17]. The kinetic and thermodynamic data of GRI-Mech 1.2 [18] (32 species and 177 chemical reactions) serves as a basis for describing the methane combustion, with iron species and reactions added as described below. Iron pentacarbonyl is added to the unburned methane/

*Certain commercial equipment, instruments, or materials are identified in this paper to adequately specify the procedure. Such identification does not imply recommendation or endorsement by the National Institute of Standards and Technology, nor does it imply that the materials or equipment are necessarily the best available for the intended use.

TABLE 1

Thermodynamic Properties of Iron-Containing Species

Species	$\Delta H_f^\circ(298)$ [kJ/mol]	$S^\circ(298)$ [J/mol-K]	$c_p(T)$ [J/mol-K] 300	400	500	600	700	800	1000	1200	1500	2000	2500	3000
$Fe(CO)_5$ [40]	−727.9	439.3	171.1	189	200.8	209.82	217.1	223.11	228.09	238.49	244.63	250.25	252.22	255.01
Fe [39]	415.3	180.4	25.69	25.52	24.89	24.23	23.6	23.14	22.51	22.18	22.22	23.22	24.69	26.19
FeO [39]	261.2	235.6	37.36	37.66	37.78	37.82	37.91	38.07	38.45	38.91	39.75	41.34	43.26	45.35
FeO_2 [39]	79.6	266.4	42.55	46.86	49.87	51.97	53.39	54.35	55.65	56.4	57.03	57.53	57.78	57.91
FeOH [39]	105.6	250.9	51.84	53.26	53.81	54.1	54.43	54.85	56.07	57.7	60.25	63.76	65.98	67.24
$Fe(OH)_2$ [39]	−303.8	286.8	84.56	89.45	91.84	93.22	94.27	95.27	97.32	99.58	102.97	108.11	112.42	116.02
Fe(O)OH [39]	17.8	279	54.1	59.71	63.64	66.4	68.45	70.04	72.47	73.47	76.36	78.66	80	80.83
FeH [38]	510.4	225.1	29.2	29.7		31.3		32.9	34.1		36.4	38.1		

oxygen/nitrogen mixture at mole fractions of up to 500 ppm. The pressure is one atmosphere.

One-dimensional counterflow diffusion flames are simulated with a numerical code developed by Smooke [19] and a one-carbon mechanism for methane oxidation [20] (17 species and 52 chemical reactions). The somewhat smaller methane mechanism captures the important chemistry of the flame, while reducing the computational time required for calculating the extinction of the counterflow flames. Iron pentacarbonyl is added to the unburned fuel or oxidizer stream at mole fractions of up to 500 ppm. The pressure is one atmosphere.

INHIBITION MECHANISM

Metallic compounds have been studied in high-temperature reacting flows for applications such as flame suppression and materials synthesis [21–28], and rates for reactions involving gas-phase metallic compounds have appeared in the literature. A compilation of reactions and rates for a variety of metals in flames can be found in Ref. [29]. In work related to flame inhibition, authors have discussed inhibition mechanisms that involve catalytic removal of H atoms by metal species (atomic, oxide, or hydroxide) [23, 25, 31, 32]. The present work is an extension of previous work [33] in which a gas-phase inhibition mechanism was developed based largely upon the work of Jensen and Jones [30]. For completeness, the mechanism has now been expanded to include a more detailed decomposition route for $Fe(CO)_5$, a more comprehensive set of iron-species reactions, as well as a different route for formation of FeO from iron atoms.

Using information in the literature and reaction analysis, we compiled a list of iron-containing species that could exist at significant concentrations in flames. In the mechanism proposed here, the $Fe(CO)_5$ decomposition products are $Fe(CO)_4$, $Fe(CO)_3$, $Fe(CO)_2$, FeCO, and Fe [34–37], and the intermediates and product species are Fe, FeO, FeOH, $Fe(OH)_2$, Fe(O)OH, FeO_2, and FeH. There is little evidence that any other iron compounds can exist at significant concentrations for conditions discussed in this paper. For the iron-containing compounds, the thermodynamic data are from Ref. [38–40], and the transport properties are estimated. For the reader's reference, these data are listed in Tables 1 and 2.

Development of Reaction Mechanism

Using the species listed above, over 100 potential reactions were considered. Analysis of reaction endothermicities and possible reaction

TABLE 2

Estimated Transport Properties for Iron-Containing Species

Species	ϵ/k_b (K)	σ(Å)
$Fe(CO)_5$	530	6.0
Fe	3,000	4.3
FeH	3,000	4.3
FeO	3,000	4.3
FeO_2	400	4.4
FeOH	400	4.4
$Fe(OH)_2$	600	4.4
Fe(O)OH	500	4.4

ϵ/k_b = Lennard-Jones potential well depth (K); σ = Lennard-Jones collision diameter (Å).

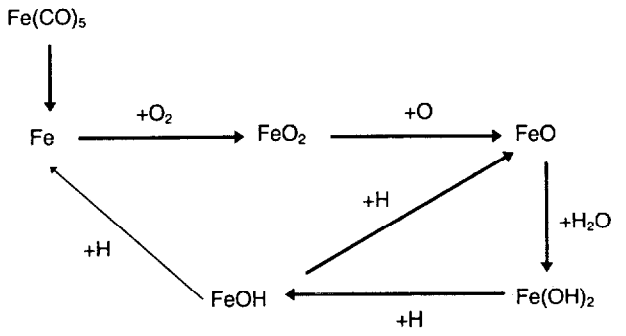

Fig. 1. Schematic diagram of reaction pathways based on the gas-phase mechanism described in this paper. Reaction partners are listed next to each arrow.

mechanisms led to the plausible set of reactions listed in Table 3, which shows the kinetic model for gaseous iron compounds at flame conditions. Rate constants were obtained from the literature or estimated using empirical procedures and reaction analogy. It was assumed that iron species are nonreactive with hydrocarbon molecules. It should be emphasized that the comprehensive set of additional reactions adopted for the present calculations should be considered only as a starting point. Numerous changes to both the rates and the reactions incorporated may be made once a variety of experimental and theoretical data are available for testing the mechanism. The reaction mechanism consists of four parts: (1) decomposition of $Fe(CO)_5$, (2) conversion of iron atoms to scavenging species, (3) scavenging of radicals through a homogeneous catalytic reaction cycle [40], and (4) reactions involving FeO_2, Fe(O)OH, and FeH. These processes are depicted in Fig. 1.

Several experiments have shown that decomposition of $Fe(CO)_5$ to Fe and CO proceeds rapidly at elevated temperatures [36, 41]. In our reaction mechanism, decomposition of $Fe(CO)_5$ involves sequential breaking of the Fe—CO bonds. Bond energies are used as the activation energies for the decomposition reactions. Rate constants of reverse reactions, independent of temperature, are taken from the literature [34, 37]. It was found that the reverse reactions proceed at a high pressure limit at one atmosphere and room temperature, and that the activation energy does not exceed 10.5 kJ/mol [37].

An important consumption reaction for iron atoms is $Fe + O_2$, and experiments have shown that the primary product of the reaction is FeO_2 [42, 43] (in previous work [33], the primary products were FeO + O [44]). The species FeO_2 is converted to FeO primarily through the reaction $FeO_2 + O \leftrightarrow FeO + O_2$, which provides one of the catalysts for the H-atom scavenging cycle

As will be described below, the inhibition mechanism is dominated by the catalytic cycle for H-atom recombination

$$FeOH + H \leftrightarrow FeO + H_2 \quad (35)$$

$$FeO + H_2O \leftrightarrow Fe(OH)_2 \quad (20)$$

$$Fe(OH)_2 + H \leftrightarrow FeOH + H_2O \quad (46)$$

$$(\text{net: } H + H \leftrightarrow H_2).$$

The cycle was developed by Jensen and Jones [30] to account for increased rates of hydrogen atom recombination in the products of rich hydrogen/oxygen/nitrogen flames with addition of $Fe(CO)_5$. Rate constants were obtained by fitting calculated H-atom concentration profiles to the experimental measurements. Although the rates for the catalytic cycle were derived from a hydrogen/oxygen flame, the sequence is likely to be applicable to a hydrocarbon flame because of the importance of hydrogen/oxygen chemistry in those flames; also, additional reactions of iron-containing species with CH_3 have been added.

RESULTS AND DISCUSSION

Premixed Flames

The decrease in the laminar burning velocity is used as a measure of the inhibition action of iron pentacarbonyl. Measurements of burning velocity are from Ref. [6], in which the average burning velocity was measured using the total area method with an accuracy of approximately ±5%, as described in detail in [6]. Because the relative change in the burning velocity could be measured with more confidence than its absolute value, the premixed flame results are presented in terms of the *normalized* burning velocity, which is defined as the burning velocity of the inhibited flame divided by the burning velocity of the uninhibited flame. For the reader's reference, the absolute calculated and measured burning velocities of the uninhibited flames are listed in Table 4 for each flame

TABLE 3 Chemical Kinetic Mechanism for Gaseous Iron Species in the Flame; $k = AT^b \exp\ [-E_a/(R\ T)]$*

	Reaction	A	b	E_a/R	Reference or Note
1	$Fe(CO)_5 \rightarrow Fe(CO)_4 + CO$	2.00E+15	0	20131	[36]
2	$Fe(CO)_4 + CO \rightarrow Fe(CO)_5$	3.50E+10	0	0	[34], [37]
3	$Fe(CO)_4 \rightarrow Fe(CO)_3 + CO$	3.00E+15	0	2516	*e*, [35]
4	$Fe(CO)_3 + CO \rightarrow Fe(CO)_4$	1.30E+13	0	0	[34], [37]
5	$Fe(CO)_3 \rightarrow Fe(CO)_2 + CO$	3.00E+15	0	16105	*e*, [35]
6	$Fe(CO)_2 + CO \rightarrow Fe(CO)_3$	1.80E+13	0	0	[34], [37]
7	$Fe(CO)_2 \rightarrow FeCO + CO$	3.00E+15	0	11575	*e*, [35]
8	$FeCO + CO \rightarrow Fe(CO)_2$	1.50E+13	0	0	*e*
9	$FeCO + M \rightarrow Fe + CO + M$	6.00E+14	0	10317	[8]
10	$Fe + CO + M \rightarrow FeCO + M$	5.00E+14	0	0	[8]
11	$FeCO + O \rightarrow Fe + CO_2$	1.00E+14	0	0	*e*
12	$Fe + O + M = FeO + M$	1.00E+17	0	0	*e*
13	$Fe + OH + M = FeOH + M$	1.00E+17	0	0	*e*
14	$Fe + H + M = FeH + M$	1.00E+15	0	0	*e*
15	$Fe + O_2 = FeO + O$	1.20E+14	0	10065	[44]
16	$Fe + O_2(+M) = FeO_2(+M)$	2.00E+13	0	0	[42], [43]
	LOW	1.50E+18	0	2013	
17	$FeO + O + M = FeO_2 + M$	1.00E+16	0	0	*e*
18	$FeO + H + M = FeOH + M$	1.00E+17	0	0	*e*
19	$FeO + OH + M = Fe(O)OH + M$	5.00E+17	0	0	*e*
20	$FeO + H_2O = Fe(OH)_2$	1.62E+13	0	0	[30]†
21	$FeO + H = Fe + OH$	1.00E+14	0	3020	*e*
22	$FeO + CH_3 = Fe + CH_3O$	1.00E+14	0	6039	*e*
23	$FeO + H_2 = Fe + H_2O$	1.00E+13	0	2516	[27], [30]
24	$FeO_2 + H + M = Fe(O)OH + M$	1.00E+17	0	0	*e*
25	$FeO_2 + H = FeO + OH$	1.00E+14	0	7549	*e*
26	$FeO_2 + OH = FeOH + O_2$	1.00E+13	0	6039	*e*
27	$FeO_2 + O = FeO + O_2$	1.50E+14	0	755	*e*
28	$FeOH + O + M = Fe(O)OH + M$	1.00E+18	0	0	*e*
29	$FeOH + OH = Fe(OH)_2$	6.00E+11	0	0	*e*
30	$FeOH + OH = FeO + H_2O$	3.00E+12	0	1007	[27]
31	$FeOH + O = Fe + HO_2$	3.00E+13	0	10569	*e*
32	$FeOH + O = FeO + OH$	5.00E+13	0	755	*e*
33	$FeOH + CH_3 = FeO + CH_4$	5.00E+13	0	755	*e*
34	$FeOH + H = Fe + H_2O$	1.20E+12	0	604	*e*
35	$FeOH + H = FeO + H_2$	1.50E+14	0	805	[30]†
36	$Fe(O)OH + H + M = Fe(OH)_2 + M$	1.00E+16	0	0	*e*
37	$Fe(O)OH + CH_3 = FeO + CH_3OH$	2.00E+13	0	2013	*e*
38	$Fe(O)OH + H = FeO + H_2O$	2.00E+13	0	0	*e*
39	$Fe(O)OH + H = FeO_2 + H_2$	5.00E+13	0	503	*e*
40	$Fe(O)OH + H = FeOH + OH$	4.00E+13	0	1007	*e*
41	$Fe(O)OH + OH = FeOH + HO_2$	3.00E+13	0	10065	*e*
42	$Fe(O)OH + OH = FeO_2 + H_2O$	5.00E+13	0	0	*e*
43	$Fe(O)OH + O = FeOH + O_2$	5.00E+13	0	0	*e*
44	$Fe(O)OH + O = FeO + HO_2$	1.00E+13	0	7046	*e*
45	$Fe(O)OH + O = FeO_2 + OH$	5.00E+13	0	0	*e*
46	$Fe(OH)_2 + H = FeOH + H_2O$	1.98E+14	0	302	[30]†
47	$Fe(OH)_2 + OH = Fe(O)OH + H_2O$	1.00E+13	0	9059	*e*
48	$Fe(OH)_2 + CH_3 = FeOH + CH_3OH$	1.00E+13	0	11575	*e*
49	$FeH + O + M = FeOH + M$	1.00E+15	0	0	*e*
50	$FeH + O_2 + M = Fe(O)OH + M$	1.00E+15	0	0	*e*
51	$FeH + O_2 = FeOH + O$	1.00E+14	0	5033	*e*
52	$FeH + H = Fe + H_2$	5.00E+13	0	0	*e*
53	$FeH + O = Fe + OH$	1.00E+14	0	0	*e*
54	$FeH + OH = Fe + H_2O$	1.00E+14	0	0	*e*
55	$FeH + CH_3 = CH_4 + Fe$	1.00E+14	0	0	*e*

e = estimation. * Units for k are cm, mole, s.

† Original recommended [30] preexponentials for reactions 20, 35, and 46 are 5.40E+12, 3.00E+13, and 6.60E+13.

TABLE 4

Calculated ($v_{o,num}$) Burning Velocities, Measured ($v_{o,exp}$, [6]) Burning Velocities, and Calculated Maximum Temperatures for the Uninhibited Methane–Oxygen–Nitrogen Premixed Flames[a]

ϕ	$X_{O_2,ox}$	$v_{o,num}$ (cm/s)	$v_{o,exp}$ (cm/s)	$T_{max,num}$ (K)
0.9	0.21	36.5	37.1 ± 1.9	2135
0.9	0.24	51.1	51.4 ± 2.6	2278
1.0	0.20	35.8	33.2 ± 1.7	2178
1.0	0.21	40.6	40.6 ± 2.0	2227
1.0	0.24	55.6	59.2 ± 3.0	2353
1.1	0.20	35.9	33.8 ± 1.7	2149
1.1	0.21	40.7	39.3 ± 2.0	2207
1.1	0.24	55.4	53.4 ± 2.7	2353

The uncertainty in equivalence ratio is 1.4%. The uncertainty in the $X_{O_2,ox}$ is 1.1%.

condition. The uncertainty of the equivalence ratio measurement is ±1.4%, the uncertainty of the oxygen mole fraction measurement is ±1.1%, and the uncertainty of the $Fe(CO)_5$ mole fraction measurement is ±4%.

Use of the original rates recommended by Jensen and Jones for reactions 20, 35, and 46 [30] results in qualitative agreement with the measurements, but the predicted inhibition (shown by the dotted line in Fig. 2) is weaker than that observed in the experiments. For example, for an initial $Fe(CO)_5$ mole fraction X_{in} of 100 ppm, the model predicts a normalized burning velocity of 0.84, while the measured value is 0.63 ± 0.044. Sensitivity analysis [15, 45] is used to examine the relative importance of the inhibition reactions for burning velocity reduction. Table 5 lists the maximum sensitivity of the burning velocity to the rate constants of the iron reactions for a stoichiometric flame with initial $Fe(CO)_5$ mole fractions of 100 ppm and 500 ppm. (The sensitivity coefficients have been normalized by the highest sensitivity coefficient, which corresponds to the reaction $H + O_2 \leftrightarrow OH + O$.) The results show that the burning rate is insensitive to the decomposition rate of $Fe(CO)_5$ and sensitive to each reaction in the catalytic cycle (reactions 20, 35, and 46) roughly equally. Numerical experiments using different rates for a one-step decomposition reaction for $Fe(CO)_5$ also indicate that the inhibition is relatively insensitive to the decomposition reaction. Likewise, the inhibition is also relatively insensitive to the reaction pathway for FeO formation from Fe.

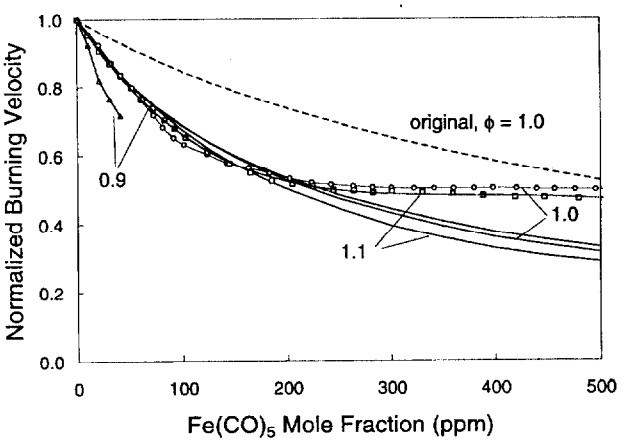

Fig. 2. Calculated and measured normalized burning velocity of premixed $CH_4/O_2/N_2$ flames with $X_{O_2,ox} = 0.21$ and varying amounts of $Fe(CO)_5$. The solid lines are the calculated normalized burning velocities using the rates in Table 3; the dashed line is the calculated normalized burning velocity using the mechanism in Table 3 with the original preexponential factors for reactions 20, 35, and 46 from Ref. [30]. Symbols are measured normalized burning velocity from Ref. [6] for $\phi = 0.9$ (triangles), $\phi = 1.0$ (circles), and $\phi = 1.1$ (squares).

The magnitude of the inhibition by $Fe(CO)_5$ is sensitive to reactions 20, 35, and 46. Increasing the preexponential term of the specific reaction rate constant by the reported uncertainties (3X, 5X, and 3X for the three reactions, respectively) increases the inhibition effect and leads to better quantitative agreement with the measurements at $\phi = 1.0$ and $X_{O_2,ox} = 0.21$ ($X_{O_2,ox}$ refers to the oxygen mole fraction in the oxidizer prior to mixing with the fuel). Such modifications to the mechanism lead to reaction rates that are nearly gas kinetic. For the remainder of the present analyses and figures, these higher values of the preexponential term are used (Table 3 shows the modified values). Some justification for the use of higher rates exists because of the possibility of condensation of iron species in the experiments of Ref. [30] (condensation will be discussed in more detail below). The temperature in the Jensen and Jones test burner (1800 to 2150 K) was such that iron species were probably supersaturated, creating the possibility of condensation; this loss of active gas-phase iron-containing molecules would have led to an underestimation of the reaction rates. Nonetheless, while use of rate

TABLE 5

First-order Sensitivity Coefficient of the Burning Velocity with Respect to Reaction Rate for Reactions with Iron-containing Species for Two Values of X_{in}, Normalized by the Peak Value for All Reactions at All Flame Locations (which Corresponds to H + $O_2 \leftrightarrow$ OH + O), and Ordered by Sensitivity Coefficient at 100 ppm[a]

No.	Reaction	$\frac{dv_0/dA_i}{dv_0/dA_i\|_{max}}$ 100 ppm	500 ppm
46	$Fe(OH)_2 + H = FeOH + H_2O$	−5.1E-02	−2.1E-01
35	$FeOH + H = FeO + H_2$	−2.8E-02	−1.0E-01
20	$FeO + H_2O = Fe(OH)_2$	−2.1E-02	−5.0E-02
32	$FeOH + O = FeO + OH$	−1.6E-02	−5.6E-02
27	$FeO_2 + O = FeO + O_2$	−1.6E-02	−5.5E-02
16	$Fe + O_2(+M) = FeO_2(+M)$	−1.4E-02	−1.9E-02
33	$FeOH + CH_3 = FeO + CH_4$	−1.2E-02	−7.8E-02
28	$FeOH + O + M = Fe(O)OH + M$	−4.6E-03	−1.8E-02
30	$FeOH + OH = FeO + H_2O$	−2.5E-03	−1.5E-02
29	$FeOH + OH = Fe(OH)_2$	−1.2E-03	−6.0E-03
13	$Fe + OH + M = FeOH + M$	−6.4E-04	−2.8E-04
24	$FeO_2 + H + M = Fe(O)OH + M$	−4.9E-04	−1.6E-03
34	$FeOH + H = Fe + H_2O$	−4.8E-04	−3.7E-03
12	$Fe + O + M = FeO + M$	−3.6E-04	−3.3E-04
25	$FeO_2 + H = FeO + OH$	−3.3E-04	−1.3E-03
42	$Fe(O)OH + OH = FeO_2 + H_2O$	−2.7E-04	−4.9E-04
18	$FeO + H + M = FeOH + M$	−1.8E-04	−2.6E-04
39	$Fe(O)OH + H = FeO_2 + H_2$	−1.7E-04	−2.1E-04
9	$FeCO + M \rightarrow Fe + CO + M$	−1.6E-04	−3.1E-04
38	$Fe(O)OH + H = FeO + H_2O$	−1.5E-04	−1.8E-04
1	$Fe(CO)_5 \rightarrow Fe(CO)_4 + CO$	−7.1E-05	−2.0E-04
48	$Fe(OH)_2 + CH_3 = FeOH + CH_3OH$	−3.2E-05	−1.1E-04
31	$FeOH + O = Fe + HO_2$	8.8E-06	−1.3E-04
19	$FeO + OH + M = Fe(O)OH + M$	1.0E-04	2.4E-04
22	$FeO + CH_3 = Fe + CH_3O$	3.4E-04	1.6E-03
26	$FeO_2 + OH = FeOH + O_2$	7.0E-04	6.1E-03
15	$Fe + O_2 = FeO + O$	7.8E-04	−1.4E-03
23	$FeO + H_2 = Fe + H_2O$	1.6E-03	3.9E-03
21	$FeO + H = Fe + OH$	2.5E-03	1.6E-03

Abbreviations: v_o = burning velocity; A_i = the preexponential of reaction i.

[a] Reactions with sensitivity coefficients with absolute values below 10^{-4} at 500 ppm are not listed.

expressions within the reported uncertainty is valid, it should be emphasized that Jensen and Jones' rate constants were deduced based on measurements in the recombination region of hydrogen/oxygen/nitrogen flames, whereas the present flames are methane/oxygen/nitrogen. Differences in the overall catalytic recombination rates caused by the iron species may be due to additional reactions in the present hydrocarbon system.

Figure 2 shows the calculated and measured normalized burning velocity as a function of initial $Fe(CO)_5$ mole fraction (X_{in}) for premixed flames with equivalence ratios of $\phi = 0.9$, 1.0, and 1.1 and $X_{O_2,ox} = 0.21$. The experimental results show strong inhibition at low X_{in} and a rather sudden leveling off of the inhibition as X_{in} increases. The numerical results are qualitatively similar to the measurements; however, the inhibition effect at low X_{in} is not as strong as that observed in the experiments (especially at $\phi = 0.9$) and at high X_{in} the inhibition effect does not diminish as dramatically as in the experiments. A complete leveling-off of the burning velocity does not occur in the simulations, even at initial $Fe(CO)_5$ mole fractions of up to 1000 ppm. Numerical tests show that better agreement at different values of ϕ can be

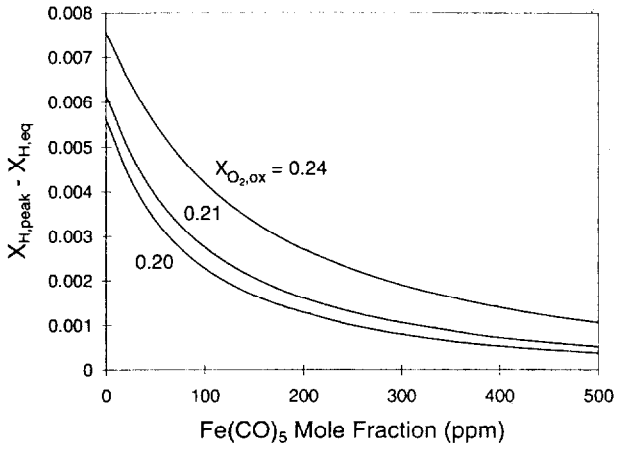

Fig. 3. Calculated dependence of superequilibrium H-atom mole fraction ($X_{H,peak} - X_{H,eq}$) on $Fe(CO)_5$ addition in premixed stoichiometric flames with $X_{O_2,ox}$ = 0.20, 0.21, and 0.24. The calculated value of $X_{H,eq}$ is approximately $2.8 \cdot 10^{-4}$ for $X_{O_2,ox}$ = 0.20, $4.1 \cdot 10^{-4}$ for $X_{O_2,ox}$ = 0.21, and $1.0 \cdot 10^{-3}$ for $X_{O_2,ox}$ = 0.24.

obtained by adjustment of reaction rates, but such fine tuning seems premature at this early stage of model development.

The decrease in the calculated inhibition effect as X_{in} increases is due to the decrease in the quantity of superequilibrium H atoms (defined as the *difference* between the peak X_H in the flame and the equilibrium X_H at the flame temperature) [6, 24, 33, 46]. This decrease can be seen in Fig. 3, where $X_{H,peak} - X_{H,eq}$ is plotted for varying X_{in} for the ϕ = 1.0 flame (the $X_{O_2,ox}$ = 0.20 and 0.24 flames are discussed below). Since the inhibition cycle (reactions 20, 35, and 46) is based on the scavenging of H radicals, the chemical effect of the inhibitor decreases with decreasing quantity of superequilibrium H atoms and a saturation effect is observed. Interestingly, halogenated flame inhibitors also show a saturation effect [47, 48], and the cause of the reduced effectiveness, reduction in radical superequilibrium, may be the same.

The effect of oxygen mole fraction on the burning velocity is presented in Fig. 4a, Fig. 4b, and Fig. 4c for ϕ = 1.0, 1.1, and 0.9. Figure 4a shows the normalized burning velocity as a function of X_{in} for ϕ = 1.0 flames with three oxidizer compositions: $X_{O_2,ox}$ = 0.20, 0.21, and 0.24. The experimental results show that as $X_{O_2,ox}$ increases, the inhibition effect decreases. As Fig. 4a–c show, the numerical model qualitatively predicts this behavior with respect to $X_{O_2,ox}$ for ϕ = 1.0, ϕ = 1.1, and ϕ = 0.9. Further, an analysis of the numerical results shows that for stoichiometric flames with 50 ppm $Fe(CO)_5$ in the reactants, the catalytic recombination mechanism accounts for 20, 19, and 15% of the total H-atom reaction flux for consumption of H, for $X_{O_2,ox}$ = 0.20, 0.21, and 0.24. That is, at higher oxygen mole fractions, the creation and destruction fluxes for hydrogen become larger, and the iron-species reactions become a smaller fraction of the total flux (for a fixed initial inhibitor mole fraction).

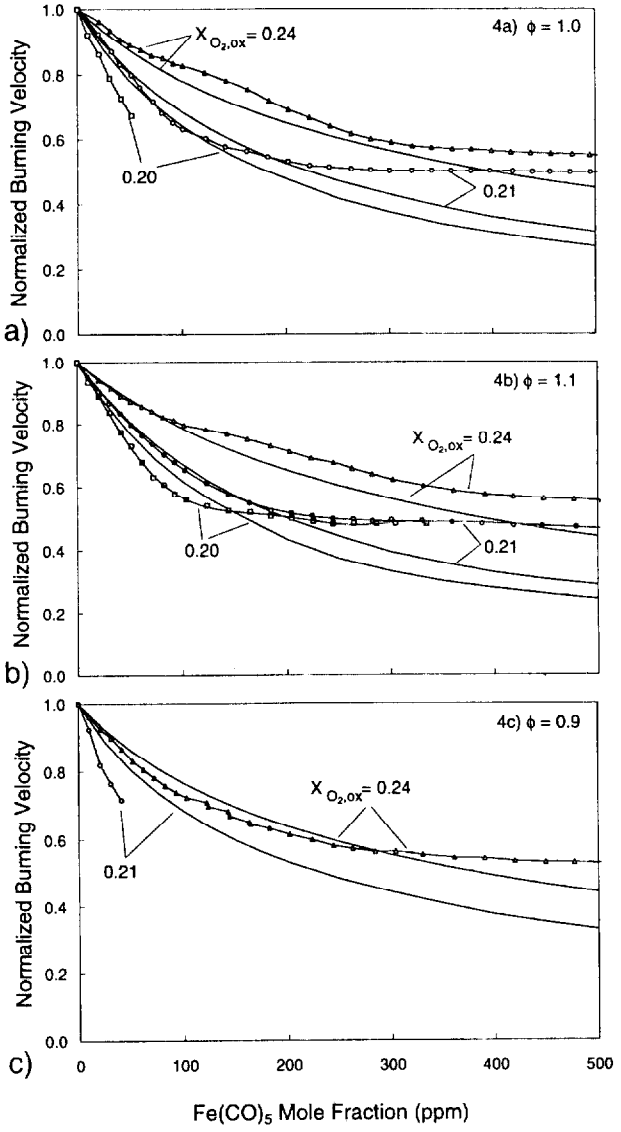

Fig. 4. Calculations and measurements of normalized burning velocity of premixed $CH_4/O_2/N_2$ flames with $X_{O_2,ox}$ = 0.20 (squares), 0.21 (circles), and 0.24 (triangles). (a) ϕ = 1.0, (b) ϕ = 1.1, and (c) ϕ = 0.9. Experimental data from Ref. [6].

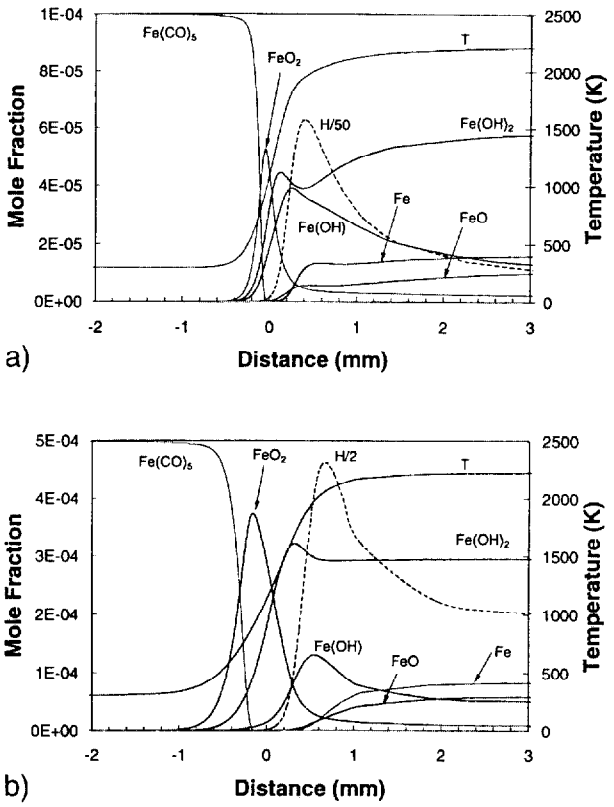

Fig. 5. Gas temperature, iron compound mole fractions, and H atom mole fraction in a $CH_4/O_2/N_2$ flame with ϕ = 1.0 and $X_{O_2,ox}$ = 0.21. (a) 100 ppm $Fe(CO)_5$. (b) 500 ppm $Fe(CO)_5$. The location of zero corresponds to the point of 50% CH_4 consumption. Note the change in mole fraction scale from (a) to (b).

Figure 5a shows calculated mole fraction profiles of the iron compounds, H-atom and temperature through the stoichiometric premixed flame with $X_{O_2,ox}$ = 0.21 and X_{in} = 100 ppm. The zero point of the x-axis is defined as the position where 50% of the CH_4 has been consumed. The mole fraction profile of $Fe(OH)_2$ exhibits a local minimum in the region of maximum H-atom mole fraction. At that location, the mole fractions of H and OH are sufficiently large so that the reactions of $Fe(OH)_2$ with H and OH proceed at a rate faster than the $Fe(OH)_2$ production reactions. Figure 5b shows similar species and temperature profiles but with X_{in} = 500 ppm. The flame thickness is increased as a result of the lower burning rate. At this higher inhibitor loading, the profile for $Fe(OH)_2$ does not show a local minimum, since with higher mole fractions of the inhibiting species, H is the limiting species in the catalytic scavenging cycle (recall from Fig. 3 the sharp decrease in X_H as X_{in} increases).

The rapid decomposition of $Fe(CO)_5$ creates the possibility of condensation of iron particles in the preheat zone of the flame. To investigate this possibility, an abbreviated kinetic nucleation model for iron atoms [8] was included in the chemical mechanism (with iron clusters up to Fe_9). The kinetic nucleation model consisted of reactions describing the growth and coagulation of iron particles. For a stoichiometric flame with X_{in} = 100 ppm, the calculations showed that some condensation occurs between the $Fe(CO)_5$-decomposition zone and the flame reaction zone, but there is not enough time for significant amounts of nucleation before the Fe reacts to form other species or the gas temperature rises to slow the nucleation rate. Not more than 5–10% of the Fe condenses and participates in nucleation reactions in the prereaction zone, which has a relatively small effect on the burning rate. This conclusion that condensation has an insignificant effect on the burning rate, however, only applies to condensation of iron atoms in the preheat region, and not to other species or other regions of the flame. For example, some of the iron particles that form in the preheat zone may vaporize, or continue to grow as they pass through the flame front. More importantly, other iron compounds may condense later in the flame.

Counterflow Diffusion Flames

Counterflow diffusion flames provide additional opportunities to study the behavior of $Fe(CO)_5$. The inhibitor can be subjected to different chemical and thermal histories by varying the reactants, the location of the inhibitor addition, and the flame location. The reduction in the extinction strain rate (a_{ext}, defined as the axial velocity gradient in the oxidizer stream at extinction) is used as a measure of the inhibition action of iron pentacarbonyl.

The counterflow diffusion flame results are presented in terms of a normalized extinction strain rate, which is defined as the ratio of the extinction strain rate of an inhibited flame to that of an uninhibited flame. The normalized value is used since Chelliah et al. [49] have shown that the absolute values of a_{ext} can depend on experimental burner design and the numerical description of the flow field, whereas

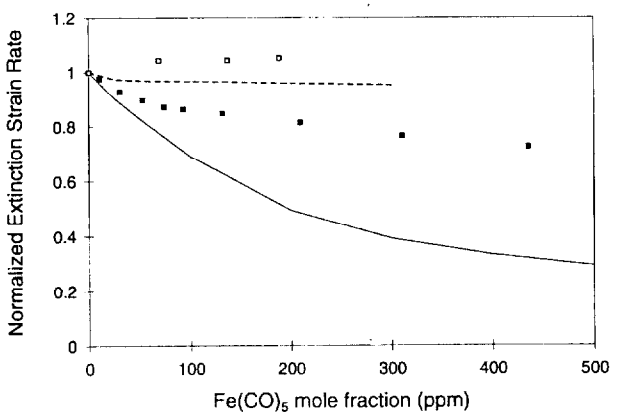

Fig. 6. Normalized extinction strain rate for counterflow diffusion flame as $Fe(CO)_5$ input varies. Closed symbols: measurements with the $Fe(CO)_5$ in the oxidizer; open symbols: measurements with $Fe(CO)_5$ in the fuel; solid line: calculations with $Fe(CO)_5$ in the oxidizer; dashed line: calculation with $Fe(CO)_5$ in the fuel. Experimental data from Ref. [6].

the trends in a_{ext} are independent of the flowfield characteristics in the experiment or model.

Figure 6 shows the measured and calculated normalized extinction strain rates for a methane/air flame with varying $Fe(CO)_5$ input. The flame is located on the oxidizer side of the stagnation plane, and the maximum temperature is approximately 1800 K at extinction. For the uninhibited flame, the measured a_{ext} is $610 \pm 30\ s^{-1}$ and the calculated a_{ext} is $520\ s^{-1}$. Experimental results [6] show that when $Fe(CO)_5$ is added to the oxidizer stream, a significant decrease in a_{ext} results. In contrast, when the $Fe(CO)_5$ is added to the fuel stream, little change in a_{ext} results. The numerical simulations qualitatively reproduce the significant dependence of inhibition on the location of $Fe(CO)_5$ addition.

The effect of $Fe(CO)_5$ on the extinction of two other counterflow flame configurations was described in Ref. [6]: (1) a flame located on the fuel side of the stagnation plane (13% CH_4/87% N_2 vs. 45% O_2/55% N_2) and (2) a flame of diluted methane located on the oxidizer side of the stagnation plane (20% CH_4/80% N_2 vs. 45% O_2/55% N_2). In these two flames, addition of $Fe(CO)_5$ to either the fuel or the oxidizer stream resulted in little reduction in a_{ext}. Calculations of a_{ext}, using the mechanism in Table 3, however, showed a significant decrease in a_{ext} as the inhibitor concentration increased for the inhibitor in either stream. The next section discusses some possible reasons for the difference.

Condensation of Iron Compounds

Figures 2 and 4 show the experimentally measured normalized burning velocity decreasing sharply at low inhibitor mole fractions but eventually leveling off at high inhibitor mole fractions. Additionally, the addition of $Fe(CO)_5$ to a counterflow diffusion flame had the strongest relative effect at low X_{in}. An explanation for the decrease in inhibition as X_{in} increases is that gaseous iron compounds—which are the primary inhibiting species—condense at higher inhibitor mole fractions, thus reducing the concentration of inhibiting species. Such behavior was discussed by Jensen and Webb [7] in numerical studies of suppression of afterburning in rocket plumes. Their calculations showed that the formation of particles in the reaction zone lowered the radical removal rate (i.e., the suppression) and led to less effective prevention of afterburning in a rocket plume as compared to the pure gas-phase effect. Further evidence of the importance of condensation can be found in the experimental data of Fig. 4a–c, which shows that as $X_{O_2,ox}$ increases for constant ϕ, the normalized burning velocity levels off at a higher value of X_{in}. Higher values of $X_{O_2,ox}$ result in higher flame temperature and higher saturation vapor pressures for the iron compounds, so that higher amounts of inhibitor are required for condensation to begin.

Figure 7 shows that there exists a potential for condensation of iron species in the $Fe(CO)_5$-inhibited premixed flame described in this paper. The figure displays the calculated supersaturation ratio (the ratio of the local mole fraction to the saturation mole fraction, $S = X/X_{sat}$) of Fe and FeO through the flame front. The saturation mole fraction was calculated from the gas temperature at each location in the flame using data from Ref. [38]. In the preheat zone of the flame, the supersaturation ratios for Fe and FeO are very high, but as the temperature increases, the saturation mole fraction increases more rapidly than the actual mole fraction, thus lowering the supersaturation ratio. Also, as X_{in} increases, the supersaturation ratio

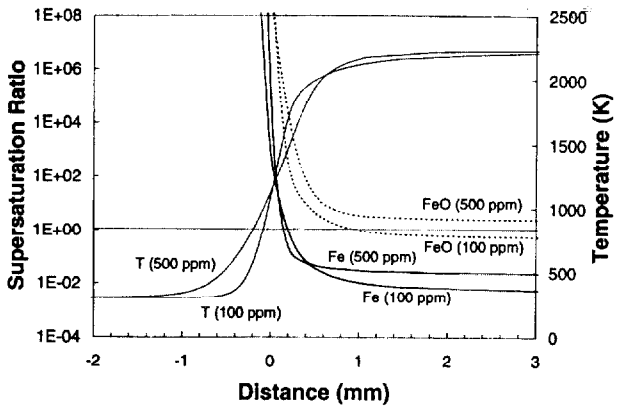

Fig. 7. Calculated supersaturation ratios ($S_i = X_i/X_{i,sat}$) for Fe (solid lines) and FeO (dashed lines) in a $\phi = 1.0$ and $X_{O_2,ox} = 0.21$ flame at $Fe(CO)_5$ concentrations of 100 ppm and 500 ppm. Note the horizontal line at $S = 1.0$ to mark the saturation point (but not necessarily the condensation point). Temperature profiles are also shown. The location of zero corresponds to the point of 50% CH_4 consumption.

increases at each location. Note that the horizontal line at $S = 1.0$ marks the saturation point, which is not necessarily the condensation point.

The critical supersaturation ratio (S_c) can be used to describe the likelihood of condensation of a supersaturated vapor. At values of S above S_c, rates of nucleation and particle growth are high, whereas below S_c, rates of nucleation and particle growth are relatively small. Frurip and Bauer [9] measured the S_c of iron vapor between 1600 K and 2200 K and found S_c values of 10 and 1000, demonstrating that supersaturation ratios greater than unity do not necessarily lead to condensation of iron vapor.

CONCLUSIONS

While the highly efficient inhibition action of metallic compounds in hydrocarbon–air flames has been known for some time, there has existed controversy in the literature as to whether the mechanism involves gas-phase or heterogeneous chemistry. This paper presents the first numerical modeling of iron pentacarbonyl's extremely strong inhibition action in Bunsen-type premixed and counterflow diffusion flames, and provides evidence that inhibition occurs primarily by homogeneous gas-phase chemistry at low initial $Fe(CO)_5$ mole fraction. While we do not believe that the present calculations explicitly rule out heterogeneous chemical effects, we believe that the proposed mechanism, based on homogeneous chemistry, can explain much—but not all—of our measurements.

Calculations using the rates constants for the catalytic cycle reactions (20, 35, and 46) suggested in Ref. [30] yield normalized burning velocities in qualitative agreement with experimental measurements; however, they predict less inhibition than was measured. Analysis of the numerical results confirms that the primary inhibition occurs through the catalytic cycle of reactions (20, 35, and 46). An increase in the rate constants (within experimental uncertainty) of reactions (20, 35, and 46) leads to improved agreement between experiments and calculations at low $Fe(CO)_5$ mole fractions for several equivalence ratios and oxygen concentrations. At higher initial $Fe(CO)_5$ mole fractions, however, the calculations predict a stronger effect than measured and do not predict the leveling off in burning velocity that was measured. Likewise, for a counterflow diffusion flame of methane flowing against air, calculations of the extinction strain rate agree with experimental measurements at low values of X_{in}, but at higher X_{in} the simulations predict a stronger effect on a_{ext} than was measured. In both cases, the reduction in $Fe(CO)_5$ effectiveness is suggested to be caused by condensation of iron-containing species when higher initial mole fractions of inhibitor are added.

Several results reported in this paper support the hypothesis that the flame inhibition effect of $Fe(CO)_5$ is primarily a result of gas-phase scavenging reactions: (1) failure of the gas-phase model to predict the leveling off of burning velocity at high X_{in}, (2) the shift of the leveling-off point (in experimental results) of normalized burning velocity to higher X_{in} as $X_{O_2,ox}$ increases (and flame temperature increases), and (3) calculated supersaturation ratios of iron compounds that are significantly higher than unity in some regions of the flames.

The performance of the present gas-phase mechanism is considered very good; nonetheless, certain experimental observations are not fully accounted for. In particular, the predicted inhibition for lean premixed flames is not strong enough, and for diffusion flames with diluted methane the calculations significantly overpre-

dict the inhibition. The range of flame temperature studied here is fairly narrow: about 2100 to 2400 K in the premixed flames and about 1800 to 2000 K in the diffusion flames. Future research will examine a wider variety of counterflow diffusion flames—which will allow greater variation in temperature and gas composition—and will measure particulate properties to elucidate the role of condensed iron compounds. More research is desirable to test the validity of the higher rates for reactions 20, 35, and 46 indicated here, and to determine if additional inhibition reactions are important in hydrocarbon flames.

The financial support of the Alexander von Humboldt Foundation for D. R. and of the Army Research Laboratory (K. McNesby and A. Miziolek) for V. B. is gratefully acknowledged. The helpful suggestions of Professor Harsha Chelliah concerning the counterflow diffusion flame calculations contributed greatly to this research, as did the generosity of Professor Mitchell Smooke for the use of his diffusion flame code. The authors also thank Mr. Newton Liu for helping with the numerical simulations and Dr. Wing Tsang for helpful discussions and suggestions.

REFERENCES

1. Lask, G., and Wagner, H. G., *Eighth Symposium (International) on Combustion*, Williams & Wilkins, Baltimore, 1962, p. 432.
2. Vanpee, M., and Shirodkar, P., *Seventeenth Symposium (International) on Combustion*, The Combustion Institute, Pittsburgh, 1979, p. 787.
3. Miller, D. R., Evers, R. L., and Skinner, G. B., *Combust. Flame* 7:137 (1963).
4. Jost, W., Bonne, U., and Wagner, H. G., *Chem. Eng. News* 39:76 (1961).
5. Bonne, U., Jost, W., and Wagner, H. G., *Fire Res. Abstracts Rev.* 4:6 (1962).
6. Reinelt, D., and Linteris, G. T., *26th Symposium (International) on Combustion*, The Combustion Institute, Pittsburgh, 1996, p. 1421.
7. Jensen, D. E., and Webb, B. C., *AIAA J.* 14:947 (1976).
8. Krestinin, A. V., Smirnov, V. N., and Zaslonko, I. S., *Khimicheskaya Fizika (Chemical Physics)* 9(3):418 (1990).
9. Frurip, D. J., and Bauer, S. H., *J. Phys. Chem.* 81(10): 1001 (1977).
10. Vree, P. H., and Miller, W. J., *Fire Res. Abstracts Rev.* 10:121 (1968).
11. McMillin, B. K., Biswas, P., and Zachariah, M. R., *J. Mater. Res.* 11(6):1552 (1996).
12. Egerton, A., and Rudrakanchana, S., *Proc. R. Soc. London* A225:427 (1954).
13. Linevsky, M. J. (1971). *Metal Oxide Studies—Iron Oxidation*. Technical Report RADC-TR-71-259.
14. Babushok, V., Tsang, W., Linteris, G., Reinelt, D., Chemical limits to flame inhibition, *Combust. Flame* (accepted for publication).
15. Kee, R. J., Grcar, J. F., Smooke, M. D., and Miller, J. A. (1991). *A Fortran Computer Program for Modeling Steady Laminar One-dimensional Premixed Flames*. Rept. SAND85-8240, Sandia National Laboratories.
16. Kee, R. J. Rupley, F. M., and Miller, J. A. (1989). *CHEMKIN-II: A Fortran Chemical Kinetics Package for the Analysis of Gas Phase Chemical Kinetics*. SAND89-8009B, Sandia National Laboratory.
17. Kee, R. J., Dixon-Lewis, G., Warnatz, J., Coltrin, R. E., and Miller, J. A. (1986). *A Fortran Computer Package for the Evaluation of Gas-Phase, Multicomponent Transport Properties*. SAND86-8246, Sandia National Laboratory.
18. Frenklach, M., Wang, H., Yu, C.-L., Goldenberg, M., Bowman, C. T., Hanson, R. K., Davidson, D. F., Chang, E. J., Smith, G. P., Golden, D. M., Gardiner, W. C., and Lissianski, V., *GRI-Mech 1.2*, http://www.me.berkeley.edu/gri_mech.
19. Smooke, M. D., Puri, I. K., and Seshadri, K., *Twenty-First Symposium (International) on Combustion*, The Combustion Institute, Pittsburgh, 1986, p. 1783.
20. Peters, N., in *Reduced Kinetic Mechanisms for Applications in Combustion Systems* (N. Peters and B. Rogg, Eds.), Springer-Verlag, New York, 1993, p. 3.
21. Erhard, K. H. L., and Norrish, R. G. W., *Proc. R. Soc. London* A234:178 (1956).
22. Norrish, R. G. W., *Seventh Symposium (International) on Combustion*, Butterworths, London, 1959, p. 203.
23. Rosser, W. A., Inami, S. H., and Wise, H., *Combust. Flame* 7:107 (1963).
24. Hastie, J. W., *High Temperature Vapors*, Academic Press, New York, 1975.
25. Friedman, R., and Levy, J. B., *Combust. Flame* 7:195 (1963).
26. Bulewicz, E. M., and Padley, P. J., *Thirteenth Symposium (International) on Combustion*, The Combustion Institute, Pittsburgh, 1971, p. 73.
27. Jensen, D. E., *J. Chem. Soc. Faraday Trans. II* 76:1494 (1980).
28. Cotton, D. H., and Jenkins, D. R., *Trans. Faraday Soc.* 67:730 (1971).
29. Jensen, D. E., and Jones, G. A., *Combust. Flame* 32:1 (1978).
30. Jensen, D. E., and Jones, G. A., *J. Chem. Phys.* 60:3421 (1974).
31. Iya, K. S., Wollowitz, S., and Kaskan, W. E., *Fifteenth Symposium (International) on Combustion*, The Combustion Institute, Pittsburgh, 1975, p. 329.
32. Birchal, J. D., *Combust. Flame* 14:85 (1970).
33. Reinelt, D., Babushok, V., and Linteris, G. T., "Numerical Study of the Inhibition of Premixed and Diffusion Flames by Iron Pentacarbonyl," Eastern States Section Meeting of The Combustion Institute, Hilton Head, SC, December 1996.

34. Seder, T. A., Ouderkirk, A. J., and Weitz, E., *J. Chem. Phys.* 85(4):1977 (1986).
35. Engelking, P. C., and Lineberger, W. C., *J. Am. Chem. Soc.* 101(19):5569 (1979).
36. Lewis, K. E., Golden, D. M., and Smith, G. P., *J. Am. Chem. Soc.* 106:3905 (1984).
37. Weitz, E., *J. Phys. Chem.* 91:3945 (1987).
38. Gmelin Handbook of Inorganic and Organometallic Chemistry (8th Edition). Fe. Supplement Vol. B1, Springer-Verlag, New York, 1991, p. 46.
39. Gurvich, L. V., Veyts, I. V., and Alcock, C. B. Eds. *Thermodynamic Properties of Individual Substances*, 3rd ed., Nauka, Moscow, 1978–1982. (NIST Special Database 5. IVTANTERMO-PC, NIST, Gaithersburg, MD 20899).
40. Chase, M. W., Jr., Davies, C. A., Downey, J. R., Jr., Frurip, D. J., McDonald, R. A., and Syverud, A. N., *JANAF Thermochemical Tables*, 3rd ed., *J. Phys. Chem. Ref. Data* 14 (Suppl. 1):1–1856 (1985).
41. Freund, H. J., and Bauer, S. H., *J. Phys. Chem.* 81(10):994 (1977).
42. Akhamadov, U. S., Zaslonko, I. S., and Smirnov, V. N., *Kinet. Catal.* 29(2):291. (Engl. transl. p. 251) (1988).
43. Helmer, M., and Plane, J. M. C., *J. Chem. Soc. Faraday Trans.* 90(3):395 (1994).
44. Fontijn, A., Kurzius, S. C., and Houghton, J. J., *Fourteenth Symposium (International) on Combustion*, The Combustion Institute, Pittsburgh, 1973, p. 167.
45. Smooke, M. D., Rabitz, H., Reuven, Y., and Dryer, F. L., *Combust. Sci. Technol.* 59:295 (1988).
46. Biordi, J. C., Lazzara, C. P., and Papp, J. F., in *Halogenated Fire Suppressants* (R. G. Gann, Ed.), American Chemical Society, Washington, DC, 1975, p. 256.
47. Linteris, G. T., and Truett, L. F., *Combust. Flame* 101:15 (1996).
48. Linteris, G. T., Burgess, D. R., Babushok, V., Zachariah, M., Westmoreland, P., and Tsang, W., *Combust. Flame* 113(1–2):164 (1998).
49. Chelliah, H. K., Law, C. K., Ueda, T., Smooke, M. D., and Williams, F. A., *Twenty-Third Symposium (International) on Combustion*, The Combustion Institute, Pittsburgh, 1991, p. 503.

Received 20 November 1997; accepted 4 March 1998